SHEAR CAPACITY OF LARGE-SCALE RC BEAMS AFFECTED BY ASR

Yasuhiro Mikata[1]*, Dean J. Deschenes[2], Oguzhan Bayrak[3]

[1]Osaka Institute of Technology, Osaka, JAPAN

[2]Simpson Gumpertz & Heger Inc., USA

[3]The University of Texas at Austin, USA

Abstract

Some reinforced concrete structures located in Houston, Texas, U.S.A., have deteriorated because of alkali–silica reaction (ASR) and/or delayed ettringite formation (DEF). In these structures, cracking and reduced concrete strength can be confirmed by inspection. The long-term performance of the affected structures in terms of their strength and serviceability becomes questionable when diagonal cracking occurs. In such a situation, it is important to clarify the time-dependent relationship between ASR deterioration and the structural performance of reinforced concrete structures affected by ASR.

In this study, the shear capacity, the relationship between the applied shear force and the deflection, and the shear crack conditions in ASR-affected specimens were evaluated experimentally and by using the finite element method. This paper compares the numerical and experimental results.

Keywords: Large-scale model, Shear capacity, Chemical prestress, ASR expansion analysis, RC beams

1 INTRODUCTION

It is important to clarify the time-dependent relationship between the deterioration caused by alkali–silica reaction (ASR) and/or delayed ettringite formation (DEF) and the structural capacity of reinforced concrete (RC) structures or elements affected by ASR. In previous studies, in the presence of triaxial confinement offered by properly detailed reinforcement, the flexural capacity of the RC members affected by ASR was not reduced in comparison with that of sound specimens, because the flexural capacity was increased by chemical prestress caused by ASR expansion [1]. However, the shear capacity and shear behavior of the RC members affected by ASR are not known to the same extent. In other words, research on the structural capacity of shear-critical elements is still very sparse.

Large-scale RC beams affected by ASR were originally tested to evaluate the shear capacity and shear behavior at the Ferguson Structural Engineering Laboratory at the University of Texas at Austin [2]. As part of collaborative research efforts between the University of Texas and Osaka Institute of Technology, a numerical assessment technique using the finite element method (FEM), which can evaluate the loading capacity of RC members affected by ASR, was developed and presented in this paper.

2 MEASUREMENT AND EXPERIMENTAL METHODS

2.1 Test variables

The values of the test variables and the properties of the concrete are given in Tables 1 and 2, respectively. The test specimens used in this study were simple RC beams with a rectangular cross section of 635 mm × 1067 mm and a total length of 8433 mm, as shown in Figures 1 and 2. The specimens were RC beams with deformed mild steel No. 11 bars (cross sectional area, A_s = 1006 mm^2, yield strength, f_{sy} = 441 MPa, Young's modulus, E_s=200 kN/mm^2, Tensile strength f_u=751 MPa, Ultimate strain, ε_u =0.0678) for longitudinal reinforcement, and No. 5 bars (A_s = 200 mm^2, f_{sy}= 448 MPa, Young's modulus, E_s=200 kN/mm^2, f_u=689 MPa, Ultimate strain, ε_u =0.0878) for shear reinforcement.

The test variables were as follows. For the specimen R1, the degree of deterioration was small, and for specimen R2, ASR-induced degradation was large. The details of the concrete mixture are given in Table 3. Of significance is the Jobe-Newman sand from El Paso, Texas, which served as the

* Correspondence to: yasuhiro.mikata@oit.ac.jp

reactive fine aggregate. In addition, the concrete mixture was dosed with 2.37 kg/m^3 of NaOH to ensure ASR reactivity.

Specimens were cured under high temperatures in excess of 70 °C to ensure eventual DEF development. The structural core temperatures of specimens R1 and R2 were maintained at over 70°C for 10 and 22 hours, respectively. Figure 3 shows the structural core temperatures of specimens. These test specimens were kept in an enclosure and were heated so as to maintain high temperatures. Subsequently, during the period of ASR development, each specimen was supplied with water by a water supply system from 8:00 pm to 8:00 am to promote this chemical degradation mechanism.

During the conditioning period, each specimen was loaded with a constant shear force, replicating service loads by using a jack and a reaction beam. The shear forces applied to the deep and sectional beams were 358 and 221 kN, respectively, which are equal to 14% and 18% of the respective beam's shear capacities, as obtained in previous shear loading tests [2]. Figure 4 shows the sustained loading conditions with water supply. For the specimens R1 and R2, the service loads were applied and water was supplied after the concrete had been aged for 254 and 221 days, respectively. The specimens were put as upside-down of Figure 1 during sustained loading and structural test.

2.2 Measurement of ASR expansion

The expansion of the structural core within the test specimens in the longitudinal and vertical directions was measured by using stainless steel rods placed within the test regions as shown in Figure 2. In addition, the strains experienced by shear reinforcement were directly measured by using short lugs that were welded to the shear reinforcement. Figure 2 shows the positions of the stainless steel rods and lugs. In an effort to gain a better understanding of the ASR-expansions, free expansions of standard concrete prisms manufactured alongside the test specimens were also measured. [2]

2.3 Structural Tests

Each specimens were conducted two separate shear tests in which they acted as sectional shear test (shear span-effective depth ratio, a/d = 3.00) and deep beam test (a/d = 1.85). The lengths of the sectional and deep beam spans were 2753 and 1697 mm, respectively, and the sectional and deep beam shear reinforcement ratios were ρ_w = 0.15% and 0.31%, respectively. Additional shear reinforcement was placed to prevent shear failure in the area between the loading points for the sectional and deep beams, as shown in Figure 2. The sectional shear test was conducted first. When the deep beam shear test was subsequently conducted, the shear failure area of the first shear test was strengthened by externally tensioned steel rods to prevent the progression of shear cracks that formed during the sectional shear test. During the structural tests, the applied loads, shear reinforcement strains, and displacements were measured. The applied load and support reactions were measured by using load cells set on the top of the support beam. The displacements were measured at the center of the specimen, the loading point, and each of the support points. The details of the structural test setup are shown in Figure 5.

3 ANALYSIS METHOD

3.1 Evaluation of the chemical prestress

The expansion of the concrete due to ASR was modeled based on damage theory. The chemical prestress is calculated by equation (1). [3] The chemical prestress before the loading test are given in Table 4.

$$\sigma(t) = (1 - \Omega)E_{c0} \cdot \left(\varepsilon_c(t) - \varepsilon_0(t)\right), \quad (1)$$

where $\sigma(t)$ is the stress due to expansion; t is the age of the concrete in days; Ω is the parameter of deterioration; E_{c0} is the initial Young's modulus; $\varepsilon_c(t)$ is the longitudinal expansion strain for beam specimens, which are confined by reinforcement; and $\varepsilon_0(t)$ is the free expansion strain for a maturity of 365 days of the ASTM C 1293 prism specimens used the same concrete as beam specimens.

The parameter of deterioration is given by equation (2)

$$\Omega = \begin{cases} 0 & \varepsilon_c(t) \le \varepsilon_{cr} \\ 1 - \left(\frac{1}{1+1000\sqrt{\varepsilon_c(t)-\varepsilon_{cr}}}\right) & \varepsilon_c(t) > \varepsilon_{cr} \end{cases} \quad (2)$$

where $\varepsilon_{cr} = f_{ct}/E_c$ is the cracking strain. f_{ct} is tensile strength, E_c is Young's modulus. This definition means that Ω is 0 for a sound specimen and approaches 1 with increasing ASR expansion.

3.2 Expression of ASR expansion

The ASR expansion stress is modeled by using DIANA which is a finite element analysis software. The ASR expansion strain is restrained by the main and shear reinforcements. The chemical prestress is applied by restraining the ASR expansion strain. The concrete element is given the thermo expansion strain as the initial strain in the FEM analysis. On the surface of the concrete at the position of the main reinforcement, the simulated chemical prestress is adjusted to be equivalent to the chemical prestress calculated from equation (1).

3.3 Model for structural loading

The shear capacity and the relationship between the load and the deflection were evaluated using the FEM. In the numerical method, to ensure consistency between the ASR expansion and loading analysis performed using the model, the loading analysis considered the initial stress due to the ASR expansion.

3.3.1 Stress–strain relationship in compression

The stress–strain relationship in compression is calculated by equation (3) [4]. The slope of the strain-softening curve changes with varying element size by balancing the compressive fracture energy in a localized element, thus avoiding a mesh size dependency. Therefore, this model is suitable for FEM analysis. Figure 6 (a) shows the stress–strain relationship in compression.

$$\sigma = \begin{cases} f'_c \left\{ \frac{2\varepsilon}{\varepsilon_p} - \left(\frac{\varepsilon}{\varepsilon_p} \right)^2 \right\} & 0 \le \varepsilon \le \varepsilon_p \\ \frac{\varepsilon - \varepsilon_u}{\varepsilon_u - \varepsilon_p} & \varepsilon_p \le \varepsilon \le \varepsilon_u \end{cases}, \quad (3)$$

where $\varepsilon_u = \frac{2G_{fc}}{f'_c L_{elm}} + \varepsilon_0$, $G_{fc} = 8.8\sqrt{f'_c}$, L_{elm} is the element size, f'_c is the compressive strength, ε_p is the strain corresponding to f'_c, and $\varepsilon_0 = \frac{\varepsilon_p}{2}$.

3.3.2 Tension-softening properties

The tension-softening curve expresses the relationship between the transferred stress and the crack width, and the area below the curve corresponds to the fracture energy, which is the energy required to form a completely opened crack of unit area. The tension-softening curve is specified by the Japan Society of Civil Engineers (JSCE) codes [5], and is shown in Figure 6 (b).

4 RESULTS

4.1 Concrete strength

To obtain the 28-day strength, the compressive strength of the specimens R1 and R2 were evaluated using test pieces. When the loading test was conducted, the compressive strength and the Young's modulus for each specimen were evaluated by core sampling from beam specimens. The properties of the concrete are listed in Table 2.

The average compressive strengths of the specimens R1 and R2, which were aged for 406 and 377 days, were approximately 68% and 58% of the 28-day strength, respectively. Thus, the compressive strength, as measured by the cores taken from the test specimens, decreased as a result of ASR.

4.2 ASR crack conditions

Figure 7 shows the ASR crack conditions in the specimens R1 and R2 acting as sectional shear test at 348 and 322 days, respectively. In each specimen, the longitudinal cracks were wider than the transverse cracks as a result of the difference in the restraining effects because the number of longitudinal reinforcements was larger than the number of shear reinforcements. For cracks wider than 0.05 mm, the crack spacing for the specimen R2 (approximately 25 mm at 322 days) was smaller than that for the specimen R1 at 348 days. At the ends of the specimen R2, the maximum crack width was 3 mm at 344 days due to the allowance of free expansion without reinforcements.

4.3 Measured values of ASR expansion

Figure 8 and 9 shows the ASR expansion for specimens R1 and R2, with the specimens acting as both deep beam and sectional shear test. For both the specimens R1 and R2, the expansion strain for the sectional shear test region was larger than that for the deep beam test region as a result of the difference between their restraining effects because the number of shear reinforcements for the

sectional shear test region was smaller than that for the deep beam test region. For the shear reinforcement strain, the expansion strain for the specimen R2 reached the yield point at approximately 250 days and was larger than that for the specimen R1. For both the deep beam test region and sectional shear test region, the expansion strain for the shear reinforcement coincided with that for the transverse core concrete. This indicates that the anchorage of the reinforcement and the strength of the bond between the concrete and the reinforcement were not deteriorated by ASR cracking.

4.4 Numerical value of ASR expansion

Figure 10 shows the longitudinal and transverse stress of R1 due to ASR expansion obtained using the numerical method before the loading test. On the surface of the concrete at the position of the main reinforcement, the chemical prestress calculated by equation (1) and measured chemical prestress which is calculated from the main reinforcement strain are given in Table 4. The 28-day Young's modulus was estimated from previous tests used same mix proportion concrete [6]. The numerical chemical prestress coincided with the measured one in the specimen R1. However, in the specimen R2, numerical value did not coincide with the measured one. The measured points of main reinforcement strain are two local points in each area of deep beam span and sectional shear span. Therefore, measured strain cannot evaluate overall reinforcement strain exactly. The chemical prestress for the ASR expansion was affected by the restraining effects of the reinforcements. For the longitudinal stress, compressive stress occurred in the lower sides of the specimens because of the restraining effects of the main reinforcement. For the transverse stress, a large compressive stress occurred because of the arrangement of the shear reinforcements. In addition, the chambers of the R1 and specimen R2 induced by the chemical prestress were 3.51 and 4.08 mm, respectively, in the centers of the specimens. This indicates that the analysis model was able to express the chemical prestress due to ASR expansion.

4.5 Shear cracking

Figure 11 and 12 shows the failure modes of the specimens R1 and R2 acting as sectional shear test. In the measurements of the specimens R1 and R2, shear cracking occurred from the loading point to the support point in the sectional shear test region. In particular, in the specimen R2, shear cracking occurred linearly from the loading point to the support point. Conversely, in the analysis, shear cracking occurred near the loading point, and longitudinal cracking occurred along the main reinforcements. Thus, the numerically obtained cracking patterns were different from the measured ones. Figure 13 and 14 shows the failure modes of the specimens R1 and R2 acting as deep beams. In the measurement, shear cracking occurred linearly from the loading point to the support point. In the analysis, the shear cracking patterns coincided with the measured ones. This indicates that the analysis model was able to predict the shear cracking pattern in the deep beams.

4.6 Shear force and deflection

Figure 15 shows the relationship between the applied shear force and the deflection of the specimen R2 acting as sectional shear test. Figure 16 shows this relationship of the specimens R1 and R2 acting as deep beams. The applied shear force and the deflection resulting from the two analysis model including or excluding the chemical prestress were indicated. In the R2 sectional shear test, the maximum applied shear force was 1569 kN, and the deflection under this maximum force was 21.1 mm. The calculated deflection values including the chemical prestress precisely corresponded with the measured deflection. However, the calculated maximum shear force including the chemical prestress overestimated the measured force, whereas the calculated maximum shear force excluding the chemical prestress underestimated the measured force.

In the R1 deep beam, the maximum applied shear force was 2311 kN, and the deflection resulting from this maximum force was 22.7 mm. The calculated maximum shear force including the chemical prestress approximately corresponded to the measured force. In the R2 deep beam, the maximum applied shear force was 2440 kN, and the deflection resulting from this maximum force was 20.9 mm. The calculated maximum shear force and deflection including the chemical prestress both coincided with the measured values. This indicates that the calculated values that included the chemical prestress were able to predict the measured maximum shear force and the corresponding deflection with sufficient accuracy. However, in specimen R2, the calculated initial stiffness which included the chemical prestress did not coincide with the measured stiffness. In the case of large chemical prestress levels, these are problem for the consistency between the ASR expansion and loading analysis performed using the model.

5 CONCLUSIONS

The main conclusions of this study are as follows:

(1) In each specimen, the longitudinal cracks were wider than the transverse cracks because of the difference in the restraining effects of longitudinal and transverse reinforcement.

(2) The measured strain in the shear reinforcement coincided with that of transverse expansion of the core concrete. Therefore, the anchorage of the shear reinforcement and the integrity of the bond between the concrete and the reinforcement were not affected by ASR degradation.

(3) The FEM analysis considered the initial stress due to ASR expansion. This consideration satisfied compatibility between the ASR expansion and structural loading.

(4) With respect to the calculated ASR expansion, a greater level of compressive stress occurred in the lower sides of the specimens because of the restraining effects of the longitudinal reinforcement. The calculated chambers of specimens R1 and R2, induced by the chemical prestress were 3.5 and 4.1 mm, respectively, at the centers of the specimens.

(5) The numerical shear cracking patterns coincided with the measured ones in the deep beams. Therefore, it is possible to conclude that the analysis model was able to simulate the internal stress distribution and mechanics of load transfer.

(6) The calculated values that included the chemical prestress were able to predict the measured maximum shear force and the corresponding deflection in deep beam test. However, in the case of large chemical prestress levels, these are problem for the consistency between the ASR expansion and loading analysis performed using the model.

6 ACKNOWLEDGMENTS

This work was supported by JSPS KAKENHI Grant number 26420442 and Texas Department of Transportation.

7 REFERENCES

[1] Mikata, Y, Shimazu, Y, Hatano, Y, and Inoue, S (2012): Flexural and shear capacity of PRC beams damaged by combined deterioration due to ASR and corrosion, Proceedings of the 14th International Conference on Alkali-Aggregate Reaction in concrete, Austin U.S.A. ICAAR.

[2] Deschenes, DJ (2009): ASR/DEF-Damaged bent caps: shear tests and Field implications, Master's thesis, University of Texas at Austin.

[3] Ueda, N, Sawabe, S, Nakamura, H, and Kunieda, M (2007): Numerical study on the expansion induced by alkali silica reaction for RC members, Journal of Japan society of civil engineers, Vol.63 No.4 pp.532-548 (in Japanese).

[4] Nakamura, H, and Higai, T (2001): Compressive Fracture Energy and Fracture Zone Length of Concrete, Modeling of Inelastic Behavior of RC Structures under Seismic Loads, ASCE, pp.471-487.

[5] JSCE (2012): Standard specification for concrete structures 2012, Design.

[6] Giannini, ER (2012): Evaluation of Concrete Structures Affected by Alkali-Silica Reaction and Delayed Ettringite Formation, Doctoral dissertation, University of Texas at Austin.

TABLE 1: Test variables.

Specimen	Deterioration degree	High-temperature curing		Starting age for applying service load and supplying water (day)	Age of concrete when conducting loading test (day)
		Holding time at more than 70 °C (h)	Maximum temperature (°C)		
R1	Small	10	86	254	373
R2	Large	22	73	221	345

TABLE 2: Properties of concrete.

Specimen	Compressive strength			Age of concrete for core sampling (day)
	28-day strength of test piece (MPa)	Strength of core sampling* (MPa)	Average for core sampling* (MPa)	
R1	35.8	24.1	24.3	406
		24.4		
R2		22.0	20.6	377
		19.2		

TABLE 3: Mix proportion of concrete.

W/C	Unit weight (kg/m³)				
	W	C	S	G	NaOH
0.57	237	415	635	875	2.37

TABLE 4: Chemical prestress (before the loading test).

Specimen	$\varepsilon_c(t)$ ($\times 10^{-6}$)	$\varepsilon_0(t)$ ($\times 10^{-6}$)	ε_{cr} ($\times 10^{-6}$)	E_{c0}* (kN/mm²)	$\sigma(t)$ (cal.) (N/mm²)	Camber (mm)	$\sigma(t)$ (mea.) (N/mm²)
R1	650	4200	99	27.2	3.95	3.5	4.00
R2	450	3800	85	27.2	4.53	4.1	6.67

* The 28-day Young's modulus was estimated from previous tests used same mix proportion concrete

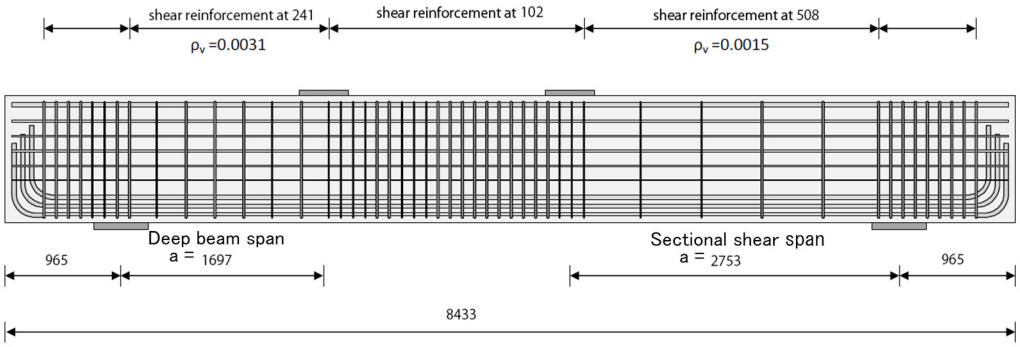

FIGURE 1: Specimen dimensions (mm) [2].

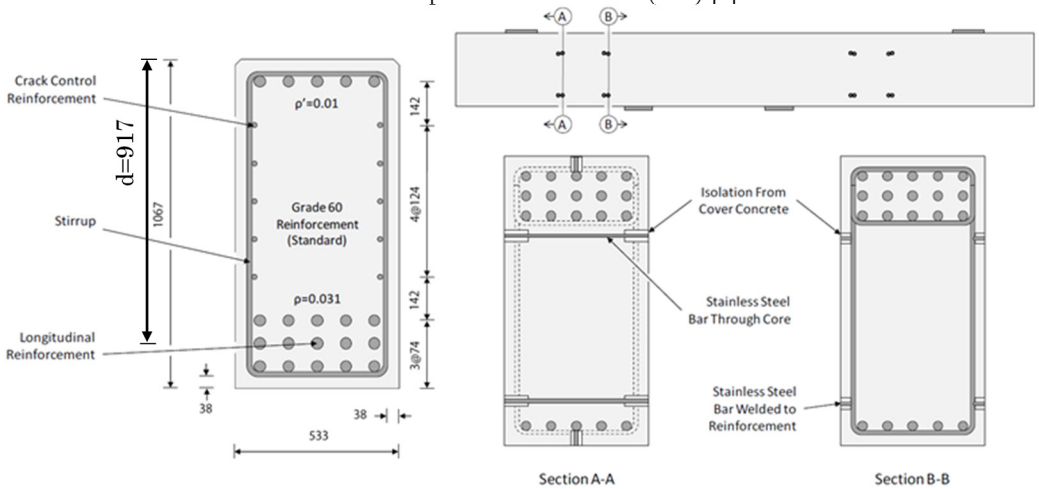

(a) Cross section (mm) (b) The position of stainless steel rods

FIGURE 2: Cross section of specimen dimensions [2].

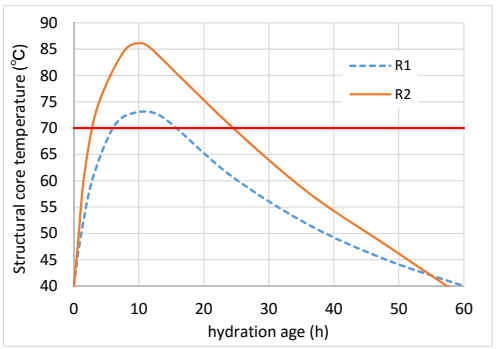

FIGURE 3: Structural core temperature [2].

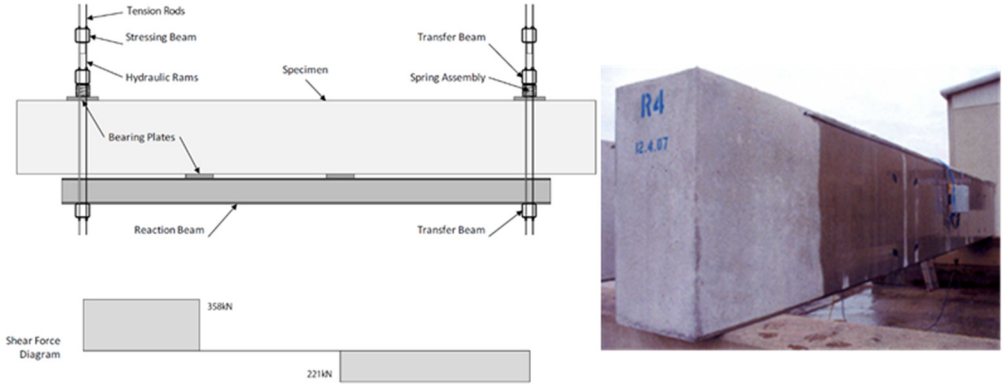

(a) Sustained loading conditions (b) Water supply system

FIGURE 4: Sustained loading conditions with water supply [2].

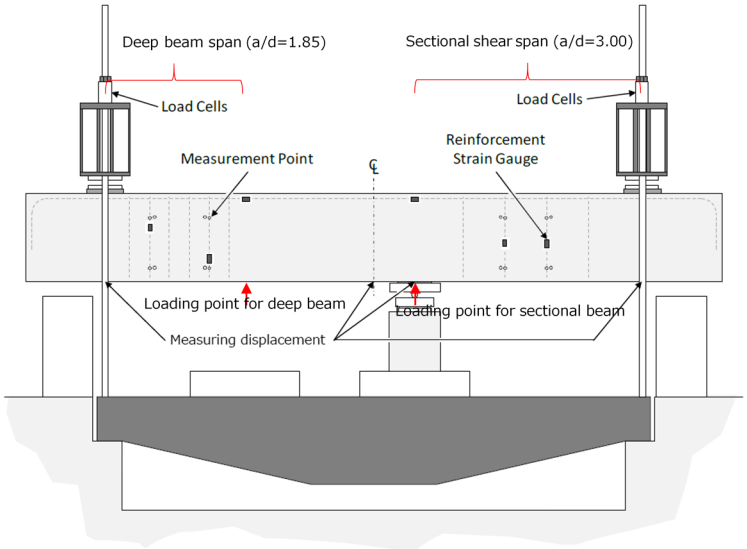

FIGURE 5: Structural Test Setup [2].

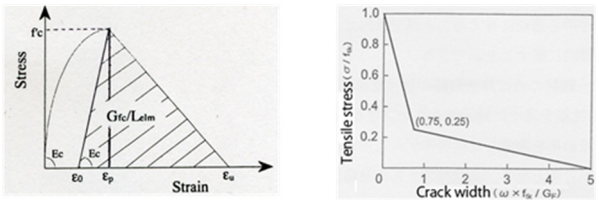

(a) Compression (b) Tension softening curve

FIGURE 6: The relationship between stress and strain.

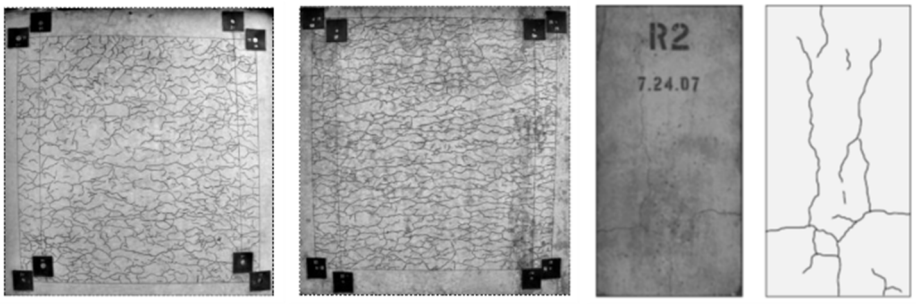

(a) Sectional beam of R1 (b) Sectional beam of R2 (c) The end face of R2

FIGURE 7: The ASR cracking condition [2].

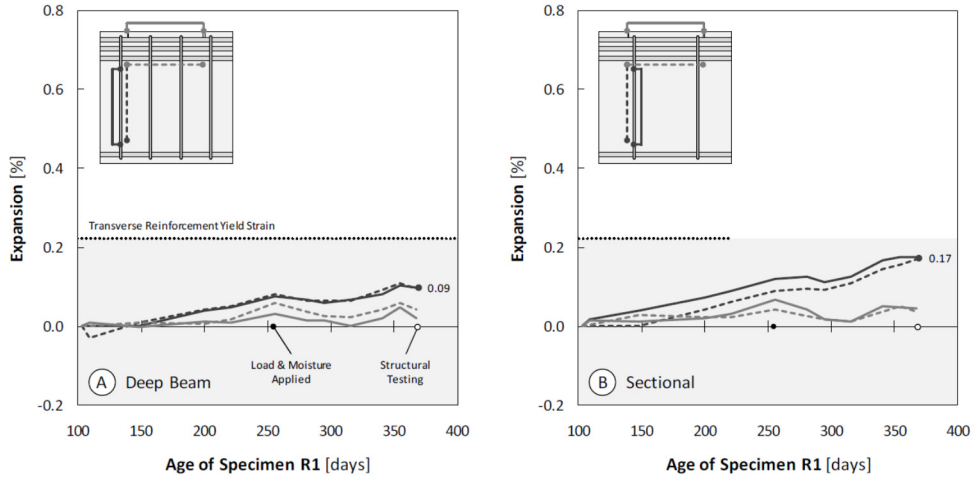

FIGURE 8: The ASR expansion (Specimen R1) [2].

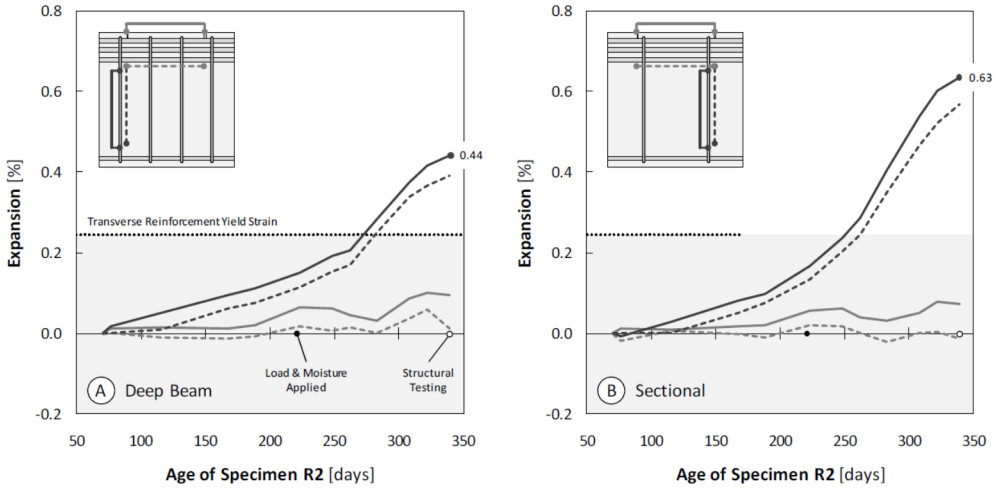

FIGURE 9: The ASR expansion (Specimen R2) [2].

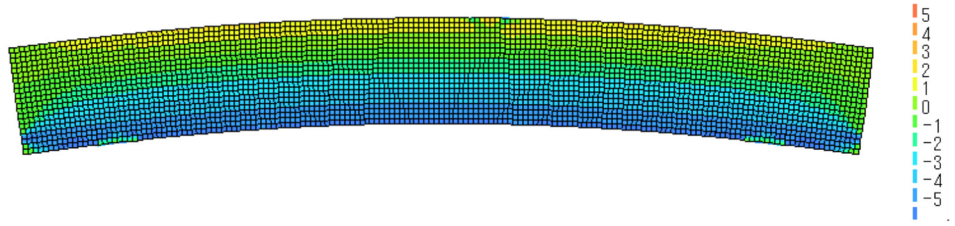

(a) Longitudinal stress

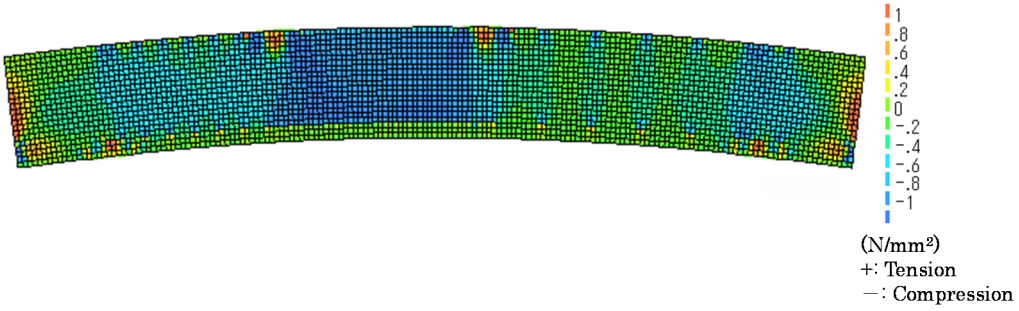

(b) Transverse stress

FIGURE 10: The longitudinal stress and the transverse stress of R1 due to ASR expansion.

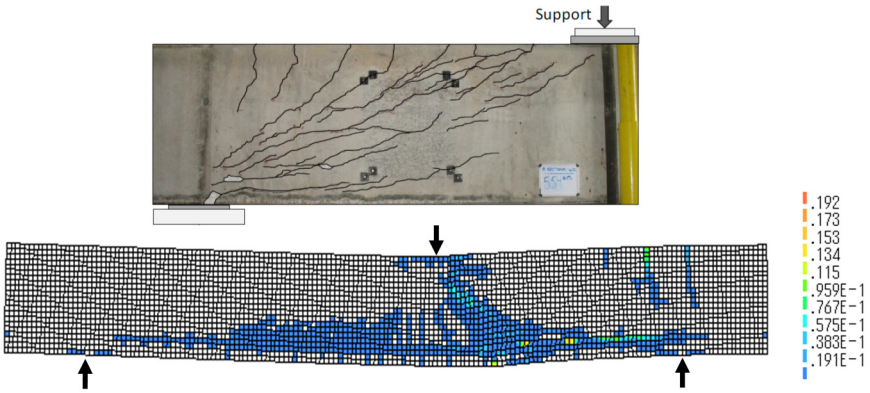

FIGURE 11: The failure mode of R1, sectional shear test region.

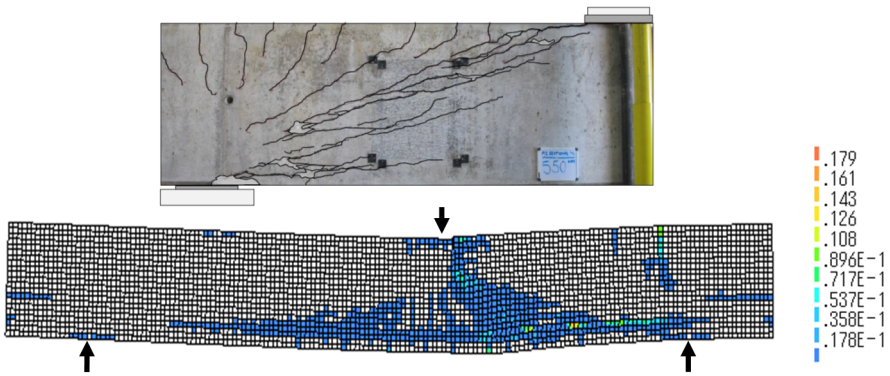

FIGURE 12: The failure mode of R2, sectional shear test region.

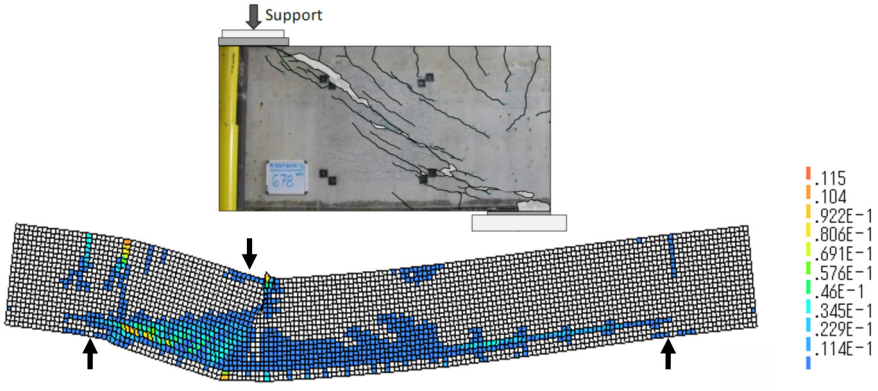

FIGURE 13: The failure mode of R1, deep beam test region.

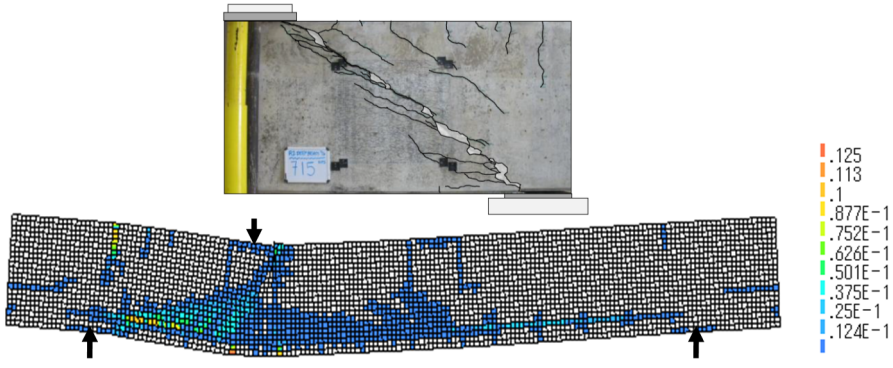

FIGURE 14: The failure mode of R2, deep beam test region.

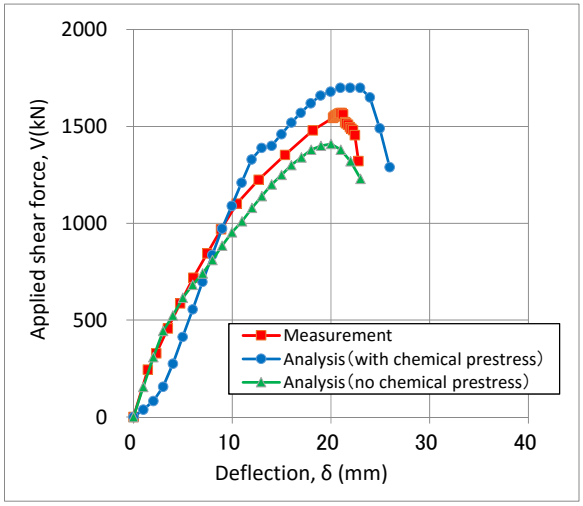

(a) Specimen R2

FIGURE 15: The relationship between applied shear force and deflection (sectional shear test).

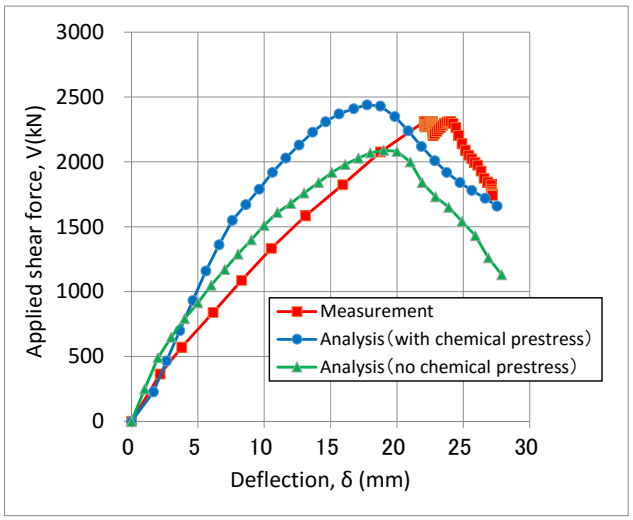

(a) Specimen R1

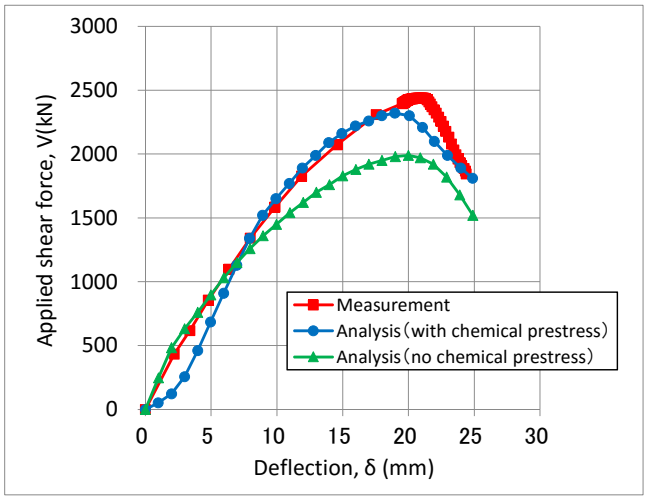

(b) Specimen R2

FIGURE 16: The relationship between applied shear force and deflection (deep beam test).